Disponible en **www.hormigonyacero.com**
Hormigón y Acero 2024
https://doi.org/10.33586/hya.2022.3087

The Influence of Flexural Reinforcement Yielding on the Shear Strength of Reinforced Concrete Beams with and without Shear Reinforcement

Influencia de la plastificación del armado a flexión en la resistencia a cortante de las vigas de hormigón armado con y sin armadura de cortante

Andrea Monserrat López[a,*], Pedro Fco. Miguel Sosa[b]

[a] *Universitat Politècnica de Catalunya, Barcelona (Spain) - Postdoctoral Margarita Salas Fellowship funded by Universitat Politècnica de València, Valencia (Spain)*

[b] *Universitat Politècnica de València, Valencia (Spain)*

Recibido el 14 de julio de 2022; revisado el 12 de septiembre de 2022, aceptado el 18 de noviembre de 2022

ABSTRACT

Statically indeterminate structures such as continuous beams allow redistribution of internal forces. For increasing loads after yielding of the flexural reinforcement, shear forces and flexural deformations may increase, making it possible to reach shear failures even after the full flexural capacity of the structure is developed.

An extensive experimental programme consisting of 30 shear tests (15 cantilever tests and 15 continuous beam tests) was carried out to assess the shear strength of reinforced concrete beams with and without shear reinforcement. Some of the tests were designed to fail in shear after yielding of the flexural reinforcement. The main objective of this experimental study was analysing the influence of large flexural strains on shear strength.

The tests were instrumented by means of surface measurements using Digital Image Correlation (DIC). These measurements allowed controlling the evolution of strains at concrete surface to obtain the rotation of the plastic hinges and tracking the development and kinematics of the critical shear crack to obtain, by accounting for suitable constitutive models, the contribution of the various shear-transfer actions.

The analysis of the test results confirmed the reduction of shear strength provided by concrete with increasing flexural rotation both in tests with and without shear reinforcement. Moreover, this shear strength component weakened for increasing shear reinforcement ratios. The test results were compared with the shear strength values predicted by different design codes, showing that these formulations did not properly capture the loss of shear strength caused by plastic deformation. The proposed simplified method to calculate the shear strength of the plastic hinges accounting for the plastic rotation demand shows consistent agreement for the experimental results.

KEYWORDS: Shear strength; reinforced concrete; shear reinforcement; continuous beam; flexural rotation; digital image correlation.

RESUMEN

Las estructuras hiperestáticas, tales como las vigas continuas, permiten la redistribución de esfuerzos internos, de forma que, tras la plastificación de la armadura de flexión, el esfuerzo cortante y la deformación pueden aumentar con el incremento de las cargas aplicadas, siendo posible alcanzar roturas por cortante incluso después de agotar la capacidad resistente por flexión de la estructura.

En este artículo se presenta un extenso programa experimental constituido por 30 ensayos de cortante (15 ensayos de voladizo y 15 ensayos de vigas continuas) llevado a cabo para evaluar la resistencia a cortante de vigas de hormigón armado con y sin armadura de cortante, algunas de ellas diseñadas para fallar a cortante tras la plastificación de la armadura de flexión. El principal objetivo de este estudio experimental era analizar la influencia del desarrollo de grandes deformaciones de flexión en la resistencia a cortante.

Durante los ensayos, se empleó la Correlación Digital de Imágenes (DIC) para obtener medidas de deformación superficiales. Estas medidas permitieron analizar la evolución de las deformaciones en la superficie de hormigón para obtener la rotación de las rótulas plásticas y hacer un seguimiento del desarrollo y la cinemática de la fisura crítica de cortante con el objetivo de obtener, considerando los modelos constitutivos adecuados, la contribución a la resistencia de los distintos mecanismos de transferencia de cortante.

El análisis de los resultados confirmó la reducción de la componente de la resistencia a cortante proporcionada por el hormigón con el aumento de la rotación de flexión, tanto en los especímenes con armadura de cortante como sin ella. Además, esta componente de la resistencia a cortante resultó menor cuanto mayor era cuantía de armadura de cortante. Los resultados se compararon con los valores de resistencia propuestos por distintos códigos de diseño, mostrando que estas formulaciones no capturan adecuadamente la reducción de resistencia a cortante causada por la deformación plástica. El método simplificado que se propone para el cálculo de la resistencia a cortante de las rótulas plásticas considerando la demanda de rotación plástica predice resultados coherentes respecto a los obtenidos experimentalmente.

PALABRAS CLAVE: resistencia a cortante; hormigón armado; armadura de cortante; viga continua; rotación de flexión; correlación digital de imágenes.

* Persona de contacto / *Corresponding author*:
Correo-e / *e-mail*: andrea.monserrat@upc.edu (Andrea Monserrat López)

How to cite this article: Monserrat, A., & Miguel, P. (2022) The influence of flexural reinforcement yielding on the shear strength of reinforced concrete beams with and without shear reinforcement, *Hormigón y Acero*, 75(302-303) https://doi.org/10.33586/hya.2022.3087

NOTATION

b concrete section width
c concrete cover
d effective depth (distance from the extreme compression fibre to the centroid of the tensile flexural reinforcement)
d_g maximum diameter of the aggregate
f_c compressive cylinder strength of concrete
f_{ct} tensile strength of concrete
f_u tensile strength of reinforcement
f_x point of the crack lip (first lip, x = 1; second lip, x = 2)
f_y yield strength of reinforcement
$l_{cont,i}$ tributary length of the crack i
l_j distance between crack i and the point j
l_k distance between crack i and the point k
l_{tot} total specimen length
l_x cantilever length (x = 1, 3) or span (x = 2)
l_{xx} segment of the span (xx = a, b, c)
m linear gradient of stress prior to yielding of reinforcement
m_y linear gradient of stress after yielding of reinforcement
s spacing of the shear reinforcement
u horizontal displacement of the crack
v vertical displacement of the crack
v_s vertical displacement related to shear deformation
w crack width normal to the crack
$\vec{w}$ crack kinematics vector
A_s area of tensile flexural reinforcement
A'_s area of compressive flexural reinforcement
A_{sw} area of shear reinforcement
M_1 absolute value of bending moment (at A support section in cantilever tests and at B support section in continuous beam tests)
M_2 bending moment (at section of applied load P_2 in continuous beam tests)
$M_{y,1}$ bending moment when flexural reinforcement is yielded at B support section
$M_{y,2}$ bending moment when flexural reinforcement is yielded at section of applied load P_2
P_x applied load (x = 1,2)
$P_{x,R}$ applied load at failure (x = 1,2)
R_A reaction in support section A
R_B reaction in support section B
V shear force
V_{agg} shear force carried by aggregate interlock
V_c shear force accounting for the sum of the various shear-transfer actions related to concrete
V_{cc} shear force carried by inclined compression chord
$V_{c,R}$ shear force at failure accounting for the sum of the various shear-transfer actions related to concrete
V_{dow} shear force carried by dowel action
$V_{dow,c}$ shear force carried by dowel action (compressive flexural reinforcement)
$V_{dow,t}$ shear force carried by dowel action (tensile flexural reinforcement)
V_E shear force applied
V_{res} shear force carried by concrete residual tensile strength
V_R shear strength
$V_{R,calc}$ estimated shear strength according to theoretical expression
$V_{R,test}$ experimental shear strength
V_s shear force carried by shear reinforcement
V_{sw} shear force carried by a stirrup
$V_{s,R}$ shear force at failure carried by shear reinforcement
V_y shear force at yielding of the flexural reinforcement
β inclination of a segment of the polyline that approximates the shape of the critical shear crack (α=180°-β)
δ crack sliding
δ_b relative concrete-to-steel slip
δ_{by} relative concrete-to-steel slip at yielding
δ_x specimen deflection under applied load (x = 1,2)
ε_{sw} strain of a stirrup
ε_u strain at maximum load of reinforcement
ε_y yield strain of reinforcement
θ angle of the critical shear crack
θ_B slope of the specimen axis at support section B
$v_{sw,i}$ vertical crack opening of the crack i at the location where it intercepts a stirrup
$v_{sw,i,SX}$ vertical crack opening at failure of the crack i at the location where it intercepts a stirrup (x =1,2,3)
ρ reinforcement ratio of flexural reinforcement
ρ_w reinforcement ratio of shear reinforcement
σ_{sw} stress of a stirrup
τ_b bond stress of reinforcement
τ_{b1} bond stress prior to yielding of reinforcement
τ_{b2} bond stress after yielding of reinforcement
ϕ nominal diameter of a reinforcing bar
χ section curvature
ψ_f flexural rotation of the specimen (general: ψ)
ψ_s rotation related to shear deformation
ψ_t total rotation of the specimen

1. INTRODUCTION

Shear behavior of reinforced concrete members has been extensively studied in recent decades and it has meant the development of extensive experimental campaigns. Mostly of these experimental studies have been focused on simply supported beams (statically determinate structures) under point loads [1,2], although many common structures, such as bridge decks or building frames are continuous beams. These structures are statically indeterminate structures with continuity and redundancy properties that allow the redistribution of internal forces. After yielding of the flexural reinforcement and with increasing loads, shear forces increase while bending moment remains almost constant in the region where the plastic hinge develops, which makes it possible for shear failures to occur after yielding of the flexural reinforcement before the full flexural capacity of the structure is developed.

The different types of shear failure –after or before yielding of the flexural reinforcement– in statically determinate and indeterminate structures are schematically illustrated in Figure 1. This figure depicts the shear-deformation path for both statically determinate and indeterminate structures and the shear failure criterion, which considers a decrease of the shear strength with increasing flexural deformation, as stated by the critical shear-crack theory (CSCT) [3]. For statically determinate structures (such as simply supported beams), members can fail in

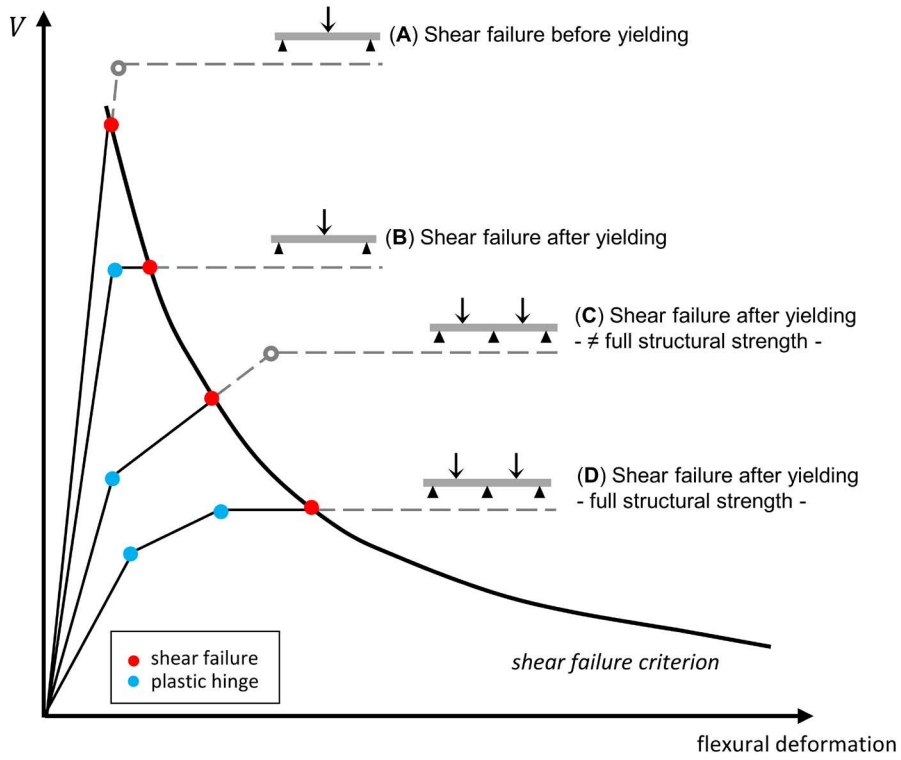

Figure 1. Structural response of structural determinate and indeterminate structures failing in shear before and after yielding of the flexural reinforcement.

shear before yielding of the flexural reinforcement (branch A in Figure 1) or after it (branch B in Figure 1). On this last case, plastic deformation develops with small load increments until the shear failure occurs. For statically indeterminate structures (such as continuous beams), members can also fail in shear before or after yielding of the flexural reinforcement. Nevertheless, in these members, load can still increase after yielding of the flexural reinforcement. As a result, members can fail in shear after yielding of the flexural reinforcement with increasing load (and increasing shear forces) –before developing the full flexural capacity of the structure– (branch C in Figure 1). After yielding, shear forces remain almost constant but the shear resistance of plastic hinges decreases for increasing flexural deformations (flexural rotation). For this reason, these members can fail in shear even though shear forces remain almost constant (branch D in Figure 1).

This structural response of statically indeterminate structures failed in shear under constant shear forces can be also understood as a reduction of the rotation capacity of plastic hinges because of shear forces, which was experimentally verified for reinforced concrete statically determinate beams without shear reinforcement failed in shear before yielding of the flexural reinforcement [3] and after this yielding [4].

Due to the lack of experimental studies focused on the shear behaviour of statically indeterminate beams –with or without stirrups– failed in shear after yielding of the flexural reinforcement and redistributing of internal forces, the authors have recently carried out an extensive experimental programme consisting of 30 shear tests aimed at representing realistic conditions of reinforced concrete structures (the experimental programme and the test results were presented and analysed in detail by Monserrat López *et al.* [5-7]). In this study, the moment-shear interaction is investigated by accounting for the influence of large flexural strains on shear strength based on displacement measurements performed by the Digital Image Correlation (DIC). To this aim, reinforced concrete members with and without shear reinforcement were tested to fail in shear under different deformation levels. In the first stage of the experimental programme (9 specimens), different flexural reinforcement ratios and configurations of load and support points were considered as the flexural rotation was the variable of study (shear reinforcement was constant for all specimens). In the second stage (6 specimens), the shear reinforcement ratio was included as a new variable of study. Although the results of this experimental programme have been previously published in other scientific papers [5-7], this paper constitutes a clear and standalone synthesis that provides the reader all required data. In addition to this summary, section 5 presents results that have not been published, constituting an original contribution of this paper.

The shear strength formulations in codes have been based on the extensive experimental and theoretical research carried out over the last decades. In this sense, design approaches have been different for members with and without shear reinforcement. While equilibrium-based models [8,9] and stress fields [10] have been developed for members with shear reinforcement, empirical formulation calibrated on the basis of experimental results (ACI 318-19 [11] and Eurocode 2 [12]) has been provided for members without shear reinforcement. Other expressions have also been extended for design of members with shear reinforcement, such as the Modified Compression Field Theory (MCFT) [13,14] (implemented in the Model Code 2010 [15] for both members

with and without shear reinforcement) or the Softened Truss Models [16,17]. For members with stirrups, design codes also have different approaches, although they share the same model, constituted by an inclined compression field and stirrups in tension. MC2010 [15] and ACI 318-19 [11] are based on adding two shear forces, a "concrete term" (V_c) and a "steel term" (V_S), referred to a section cut of these stress fields at the angle of the critical shear crack. Nevertheless, EC-2 [12] only considers a "steel term" (V_S), the shear force provided by the stirrups referred to a section cut performed parallel to the compression field. In EC-2 formulation, the shear strength contribution provided by concrete is indirectly taken into account with a variable-angle of the compression field. As far as the moment-shear interaction concerned, it is considered in the shear formulation proposed by the MC2010 [15] by a reduction of the shear strength because of the presence of a concomitant bending moment. This formulation has proven the capability of accurately predicting shear behaviour of reinforced concrete members [14]. On the contrary, other design codes such as ACI 318-19 [11] and EC-2 [12] provide empirical shear formulation for beams without stirrups which depends on the longitudinal tension reinforcement area. Unlike the previous one, this formulation has proven to be unable to properly capture the influence of different variables on the shear strength [1].

In this paper, the experimental results of the aforementioned experimental programme as well as an analysis of the shear strength according to the flexural and shear deformations is provided. Consequently, the shear failure criterion proposed by Vaz Rodriguez *et al* [4] is verified to be applicable to beams with and without shear reinforcement and for flexural rotations beyond the elastic behaviour. Based on this failure criterion, a simplified method is proposed to calculate the shear strength of the plastic hinges accounting for the plastic rotation demand.

2. EXPERIMENTAL PROGRAMME

2.1. Specimens

The experimental programme was presented in detail in Monserrat López *et al.* [5,6]. It involved 15 reinforced concrete beams and 30 shear tests. Specimens B1 to B9 were 9.00 m long (first stage of the experimental programme) and B10 to B15 were 7.00 m long (second stage of the experimental programme). All specimens had rectangular cross section of 250 x 450 mm. Two different shear tests were conducted on

TABLE 1.
Reinforcement, geometry and material properties of all tests.

Specimen	Tests	A_S	A'_S	ρ (%)	A_{SW}	ρ_W (%)	l_{tot} (m)	l_1 (m)	l_2 (m)	l_3 (m)	l_a (m)	l_b (m)	l_c (m)	f_c (MPa)	f_{ct} (MPa)
B1	B1C-R1-S1-L1 B1S-R1-S1-L6	520	720	1.63	8/30	0.13	9.00	1.00	6.00	1.00	1.00	3.10	1.90	24.1	2.5
B2	B2C-R1-S2-L1 B2S-R1-S2-L6	720	520	2.29	8/30	0.13	9.00	1.00	6.00	1.00	1.00	2.50	2.50	22.3	3.1
B3	B3C-R1-S3-L1 B3S-R1-S3-L6	620	620	1.94	8/30	0.13	9.00	1.00	6.00	1.00	1.00	2.80	2.20	22.8	2.8
B4	B4C-R1-S1-L1.6 B4S-R1-S1-L5	520	720	1.63	8/30	0.13	9.00	1.62	5.00	1.00	1.00	2.10	1.90	22.3	2.6
B5	B5C-R1-S2-L1.6 B5S-R1-S2-L5	720	520	2.29	8/30	0.13	9.00	1.62	5.00	1.00	1.00	1.50	2.50	34.7	3.6
B6	B6C-R1-S3-L1.6 B6S-R1-S3-L5	620	620	1.94	8/30	0.13	9.00	1.62	5.00	1.00	1.00	1.80	2.20	35.9	3.3
B7	B7C-R1-S1-L2.3 B7S-R1-S1-L4	520	720	1.63	8/30	0.13	9.00	2.31	4.00	1.00	1.00	1.10	1.90	36.2	2.9
B8	B8C-R1-S2-L2.3 B8S-R1-S2-L4	720	520	2.29	8/30	0.13	9.00	2.31	4.00	1.00	1.00	0.50	2.50	34.5	3.4
B9	B9C-R1-S3-L2.3 B9S-R1-S3-L4	620	620	1.94	8/30	0.13	9.00	2.31	4.00	1.00	1.00	0.80	2.20	29.7	2.2
B10	B10C-R0-S1-L1 B10S-R0-S1-L4	520	720	1.63	-	-	7.00	1.00	4.00	1.00	0.70	1.40	1.90	36.4	2.1
B11	B11C-R0-S2-L1 B11S-R0-S2-L4	720	520	2.29	-	-	7.00	1.00	4.00	1.00	1.00	0.61	2.50	31.4	2.1
B12	B12C-R0-S3-L1 B12S-R0-S3-L4	620	620	1.94	-	-	7.00	1.00	4.00	1.00	0.89	0.91	2.20	28.7	2.9
B13	B13C-R2-S1-L1 B13S-R2-S1-L4	520	720	1.63	8/20	0.20	7.00	1.00	4.00	1.00	1.00	1.10	1.90	30.6	2.5
B14	B14C-R2-S2-L1 B14S-R2-S2-L4	720	520	2.29	8/20	0.20	7.00	1.00	4.00	1.00	1.00	0.50	2.50	31.4	2.9
B15	B15C-R2-S3-L1 B15S-R2-S3-L4	620	620	1.94	8/20	0.20	7.00	1.00	4.00	1.00	1.00	0.80	2.20	26.0	2.6

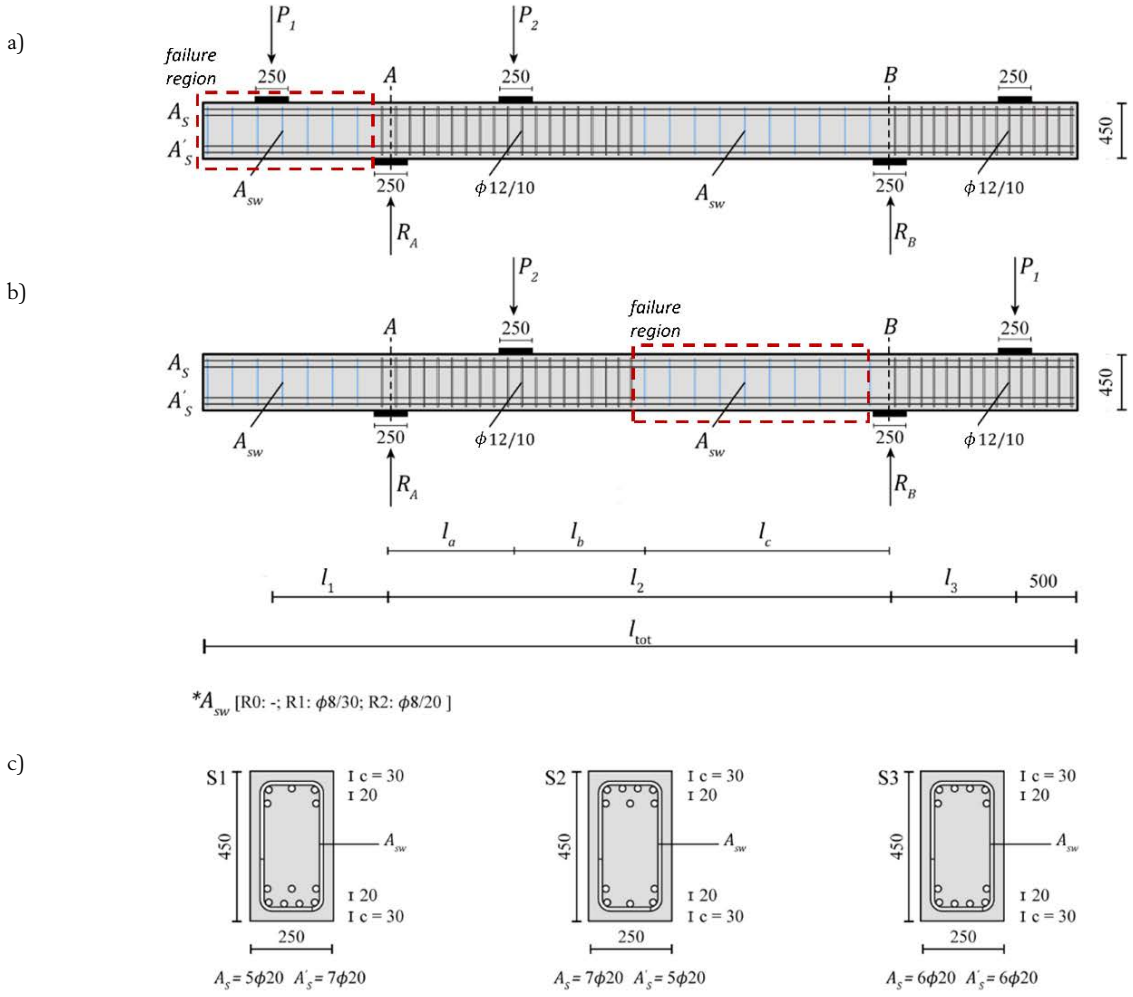

Figure 2. Reinforcement, geometry and load arrangement of the specimens in (a) cantilever test and (b) continuous beam test; (c) flexural reinforcement of section type S1 (specimens B1, B4, B7, B10 and B13), S2 (specimens B2, B5, B8, B11 and B14) and S3 (specimens B3, B6, B9, B12 and B15) (dimensions in mm).

each specimen according to different load configuration and test procedure (30 tests): test on cantilevers (Figure 2a) and test on continuous beam test (Figure 2b).

The specimens making up the first stage of the experimental programme (specimens B1 to B9) had different flexural reinforcement ratios and configurations of load and support points to allow reaching shear failures under different deformation levels (accounted by the flexural rotation). The shear reinforcement ratio was fixed in all specimens. In the second stage (specimens B10 to B15), shear reinforcement was included as a variable to study its influence in the shear behaviour of the specimens.

Three different flexural reinforcement ratios were considered (tensile top flexural reinforcement): ρ = 1.63% (section S1, effective depth d = 386 mm); ρ = 2.29% (section S2, effective depth d = 385 mm); ρ = 1.94% (section S3, effective depth d = 389 mm). All sections had a total of twelve 20 mm-diameter bars arranged as tensile (top) and compressive (bottom) flexural reinforcement (arranged in two layers, see Figure 2c) and constant along the length of the specimen. The different load and support configurations determined the length of the cantilever (l_1) in the cantilever tests and the length of the span (l_2) in the continuous beam tests. In the former l_1 was 1.00 m (L1), 1.62 m (L1.6) and 2.31 m (L2.3) (see Figure 2a); in the latter l_2 was 6.00 m (L6), 5.00 m (L5) and 4.00 m (L4) (see Figure 2b). Three series were considered with respect to the shear reinforcement: beams without shear reinforcement (series R0); beams with a shear reinforcement ratio ρ_w = 0.13% (series R1, two-legged closed stirrups ϕ8/30) and beams with a shear reinforcement ratio ρ_w = 0.20% (series R2, two-legged closed stirrups ϕ8/20). Outside of the expected failure regions, stirrups were provided to prevent shear failures (ρ_w = 0.90% in all specimens). Table 1 summarizes the reinforcement, geometry and material properties of all tests (C –cantilever– refers to the cantilever test and S –span– to the continuous beam tests).

2.2. Test system

Loads (P_1 and P_2) and support reactions (R_A and R_B) (see Figure 2a and 2b) were transmitted to the beam through steel plates measuring 250 x 250 x 40 mm. Both load and support systems allowed horizontal in-plane displacements and rotations (see Figure 3a and 3b). One of the supports of the specimens had restrained horizontal displacement during tests.

In cantilever tests (Figure 2a), load was applied with displacement control (0.02 mm/s) until shear failure, and P_2

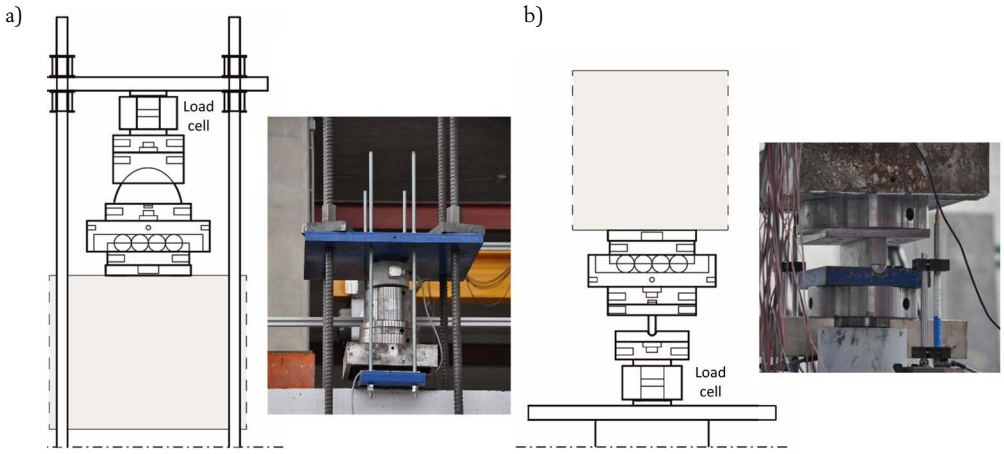

Figure 3. (a) Load system; (b) support system.

was applied with load control according to P_1 to obtain no reaction in support B. In these tests, shear force and bending moment increased simultaneously along the cantilever (l_1).

The continuous beam tests (Figure 2b) were carried out in two phases. In the first phase (Figure 4a), load P_1 was applied with displacement control (0.02 mm/s), and load P_2 with load control according to P_1 to obtain no reaction at support A. This phase ended when the top flexural reinforcement at the support B section yielded. In the second phase (Figure 4b), load P_2 was applied with displacement control (0.02 mm/s) until shear failure, and load P_1 was applied with load control to keep the slope of the specimen axis at the support B (θ_B) constant and equal to the one at the end of the first phase. It must be pointed out that specimens became statically indeterminate structures (continuous beams) in the second phase of the tests, as efforts were determined by compatibility conditions because of the restriction imposed to the slope at the support B section. Precisely this restriction allowed increasing shear force along the inner span (l_2) together with increasing flexural rotations at the plastic hinge at the support B section (plastic moment remained constant at this section). This restriction is not equivalent to keeping constant load P_1, which would result in a constant bending moment imposed at the support B section but in a decrease of rotation with increasing shear forces. Actually, it was observed that a limited increase of load P_1 was required to maintain the slope due to the increasing rotation of the plastic hinge.

2.3. *Instrumentation*

Conventional instrumentation consisted of four load cells (see Figure 3) taking continuous measurements of the two loads applied by two independent hydraulic jacks and the reactions at the support sections. In addition, several concrete displacement and strain measurements were recorded by means of displacement transducers and strain gauges [6]. The deflection of the specimens was measured at load sections by absolute non-contact position sensors integrated into hydraulic jacks and at several points of the specimens' bottom surface by displacement transducers. Two displacement transducers were used to control the slope at support sections.

In addition to these conventional measurements, two-dimensional Digital Image Correlation (DIC) was used to track the displacement field of the specimens continuously during tests. Photogrammetry was performed on the region of the specimens where shear failure was expected. Canon EOS 5D Mark II digital cameras (21.1 megapixels) equipped with a fixed-focus lens Canon EF 85 mm f/1.8 USM were used (three or four cameras depending on the test). The image acquisition rate during tests was variable. Images were taken every two seconds at the beginning, but the frequency increased up to 1 Hz near failure. In the measurement regions, a pattern consisting of rounded black speckles was applied. An own software developed using NI-IMAQ driver and programming with LabVIEW was used to obtain the isolated displacement measurements at several points of the concrete

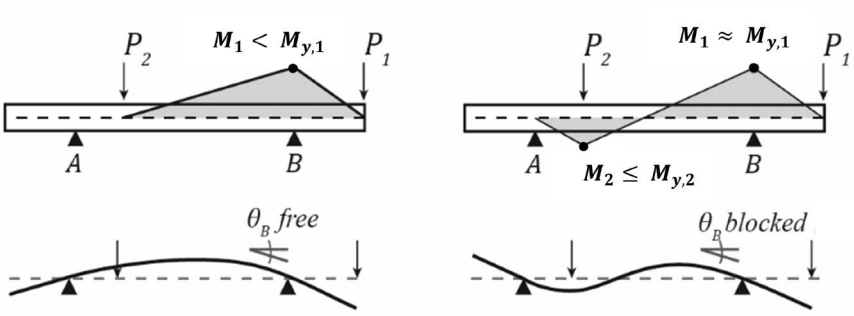

Figure 4. Bending moment diagrams for the continuous beam tests: (a) first phase of the test; (b) second phase of the test.

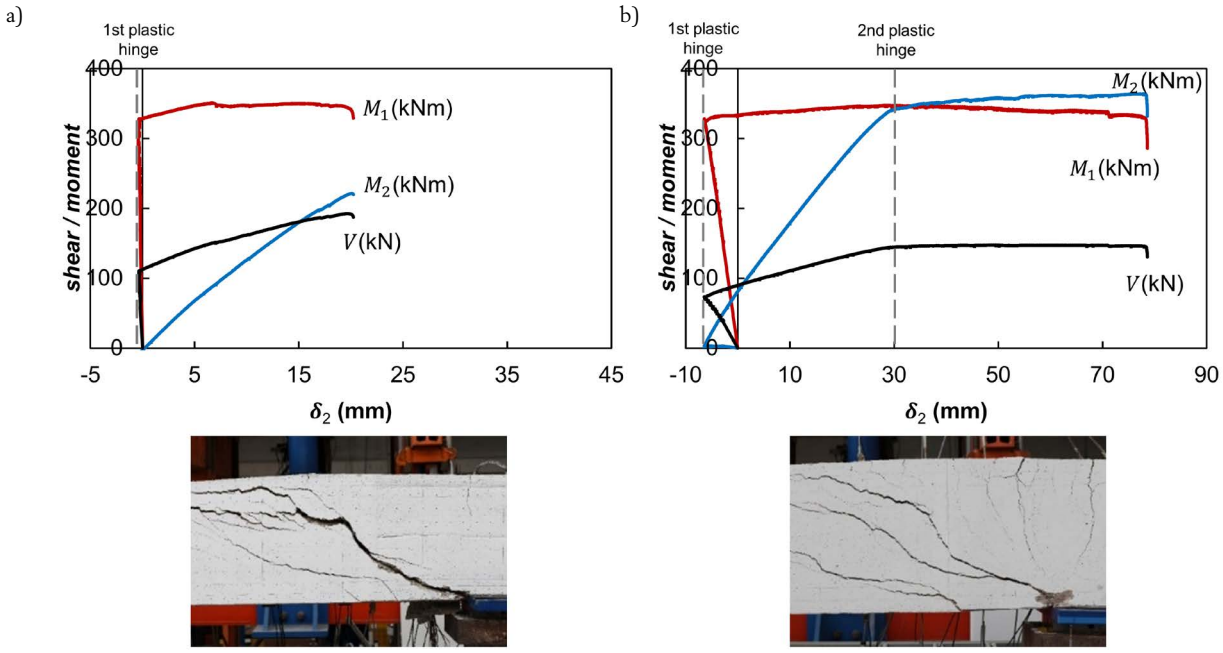

Figure 5. Evolution of the bending moments (M_1 at M_2 support section and at section of applied load P_2) and shear force (V) according to the specimen deflection P_2 under the load for the continuous beam tests: (a) B9S-R1-S3-L4; (b) B3S-R1-S3-L6.

surface. For measuring displacements, images were divided into a grid of squared facets of 100 x 100 pixels and each one was tracked from one image to the following. The software maximum error of the computed displacements was 1/32 pixels and the resolution of the calibration performed with the Vision Assistant of National Instruments software was 0.2 mm/pixel. Besides these measurements, the displacement field measurements associated with cracking development was obtained with VIC2D software [18].

3. MAIN TEST RESULTS

3.1. *Failure modes and shear strength*

Several shear failure modes were observed for the cantilever tests and the continuous beam tests.

In cantilever tests, specimens L1 and L1.6 failed in shear before yielding of the top flexural reinforcement at the support section A (see Figure 2a) with increasing shear force and bending moment. However, specimens of the tests B8C-R1-S2-L2.3 and B9C-R1-S3-L2.3 failed in shear after yielding of the top flexural reinforcement. In these cases, shear failure occurred under constant shear force but for increasing deformations. Finally, test B7C-R1-S1-L2.3 failed in bending.

In continuous beam tests, all specimens failed in shear in the second phase of loading, after yielding of the top flexural reinforcement at support section B (see Figure 2b) and the development of large rotations of the plastic hinge. Two different failure modes were observed depending on the development or not of a second plastic hinge under load P_2 (see Figure 2b). Specimens L4, and specimen of the test B4S-R1-S1-L5 failed in shear after formation of first plastic hinge with increasing shear forces and increasing flexural rotations at the plastic hinge. Specimens L6, and specimens of the tests B5S-R1-S2-L5 and B6S-R1-S3-L5 failed in shear after formation of second plastic hinge. In these cases, shear failure occurred under constant shear force but for increasing flexural rotations at the plastic hinge. Figure 5 shows the evolution of the bending moments M_1 and M_2 (absolute value of bending moment at B support section and at section of applied load P_2, respectively) and the shear force V (absolute value of shear force at B support section) according to the deflection δ_2 (specimen deflection under the load P_2) for the two different failure modes observed for the continuous beam tests (test B9S-R1-S3-L4 failed in shear after formation of first plastic hinge, see Figure 5a; and test B3S-R1-S3-L6 failed in shear after formation of second plastic hinge, see Figure 5b). The graphics show a first branch with negative slope and a limited force values, which corresponds to the first phase of the continuous beam tests.

The load-deflection curves for the specimens of series R1 (ρ_w = 0.13%) and section S3 (ρ = 1.94%) are plotted in Figure 6 (load P_1 against the deflection under this load δ_1 for cantilever tests, see Figure 6a; and load P_2 against the deflection under this load δ_2 for continuous beam tests, see Figure 6b).

Table 2 summarizes the main results of all tests at failure. It includes the failure mode, the applied loads at failure ($P_{1,R}$ for cantilever tests and $P_{1,R}$ and $P_{2,R}$ for continuous beam tests) and the shear strength (V_R) provided by tests at failure at the corresponding support section (support section A –cantilever side– for cantilever tests, see Figure 2a; and support section B –midspan side– for continuous beam tests (see Figure 2b).

3.2. *Cracking pattern*

Regarding the cracking pattern at failure, it is different for cantilever tests and continuous beam tests. In all cantilever tests,

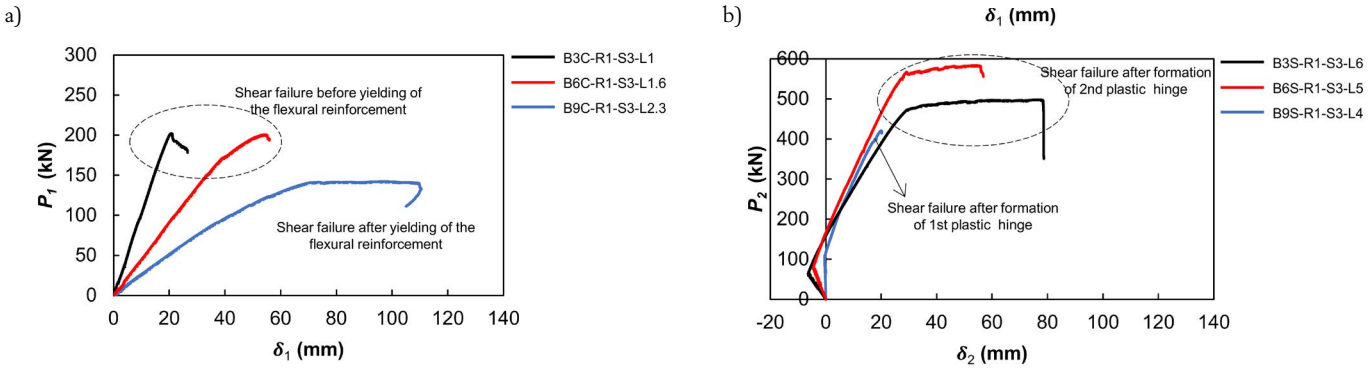

Figure 6. Load-deflection curves for the specimens of series R1 and section S3: (a) cantilever tests; (b) continuous beam tests.

TABLE 2.
Reinforcement, geometry and material properties of all tests.

Specimen	Test	Failure mode	$P_{1,R}$ (kN)	V_R (kN)	Test	Failure mode	$P_{1,R}$ (kN)	$P_{2,R}$ (kN)	V_R (kN)
B1	B1C-R1-S1-L1	V (B)	192.6	196.8	B1S-R1-S1-L6	V (2PH)	272.6	513.2	139.4
B2	B2C-R1-S2-L1	V (B)	210.4	214.6	B2S-R1-S2-L6	V (2PH)	371.4	432.3	142.4
B3	B3C-R1-S3-L1	V (B)	202.1	206.3	B3S-R1-S3-L6	V (2PH)	324.4	495.8	145.1
B4	B4C-R1-S1-L1.6	V (B)	167.2	174.2	B4S-R1-S1-L5	V (1PH)	270.2	415.5	143.1
B5	B5C-R1-S2-L1.6	V (B)	208.1	215.2	B5S-R1-S2-L5	V (2PH)	374.1	540.1	188.7
B6	B6C-R1-S3-L1.6	V (B)	200.6	207.6	B6S-R1-S3-L5	V (2PH)	343.3	581.2	190.8
B7	B7C-R1-S1-L2.3	M	120.0	-	B7S-R1-S1-L4	V (1PH)	293.7	563.1	216.3
B8	B8C-R1-S2-L2.3	V (A)	157.8	167.6	B8S-R1-S2-L4	V (1PH)	389.6	405.6	200.9
B9	B9C-R1-S3-L2.3	V (A)	138.8	148.7	B9S-R1-S3-L4	V (1PH)	341.2	419.6	192.3
B10	B10C-R0-S1-L1	V (B)	146.0	150.2	B10S-R0-S1-L4	V (1PH)	224.2	118.1	82.4
B11	B11C-R0-S2-L1	V (B)	184.7	188.9	B11S-R0-S2-L4*	V (1PH)	363.7	94.7	92.0
B12	B12C-R0-S3-L1	V (B)	116.6	120.8	B12S-R0-S3-L4	V (1PH)	241.5	97.0	87.6
B13	B13C-R2-S1-L1	V (B)	230.8	235.0	B13S-R2-S1-L4	V (1PH)	290.6	557.2	217.6
B14	B14C-R2-S2-L1	V (B)	263.5	267.7	B14S-R2-S2-L4	V (1PH)	353.5	513.8	222.5
B15	B15C-R2-S3-L1	V (B)	276.8	281.0	B15S-R2-S3-L4	V (1PH)	310.5	463.4	199.1

Note: V (shear failure); M (bending failure); A (after yielding); B (before yielding); PH (plastic hinge); shear at corresponding support section including self-weight; *test with different configuration [16].

cracking first started as vertical flexural cracks near the support section. In several tests, as load increased, one of those flexural cracks developed sub-horizontal branches (towards the support section firstly and towards the load section secondly) becoming the critical shear crack (see Figure 7a). Nevertheless, the critical shear crack developed directly as a diagonal crack in the web with increasing opening until shear failure in some L1 tests (B3C-R1-S3-L1, B11C-R0-S2-L1, B12C-R0-S3-L1 and B15C-R2-S3-L1, see Figure 7b). In continuous beam tests, the two different phases of the test influenced the evolution of the cracking pattern. In the first loading phase, mainly flexural cracking was observed, while cracking associated to shear deformations barely developed because of the limited shear forces. In the second phase, flexural cracks near to support section considerably increased and the critical shear crack progressed from a flexural crack by developing sub-horizontal branches. In general, the cracking pattern was influenced by the shear reinforcement: specimens with stirrups (series R1 and R2) exhibited more distributed cracking and larger crack openings (associated to a significant vertical displacement) than those specimens without stirrups (series R0). The observed cracking patterns for all tests were presented in detail in Monserrat López *et al.* [7].

4. ANALYSIS OF TEST RESULTS

4.1. Shear strength contributions

The contribution of the various shear-transfer actions to the shear strength can be estimated by using the kinematics associated to cracking and suitable constitutive models. For

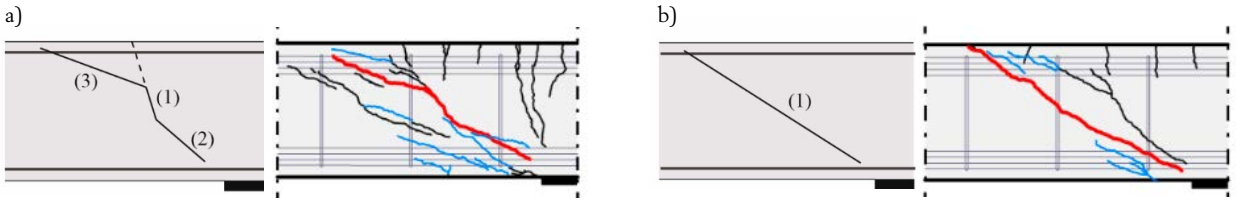

Figure 7. Crack development process: (a) critical shear crack from a flexural crack (B2C-R1-S2-L1); (b) critical shear crack as a diagonal crack in the web (B3C-R1-S3-L).

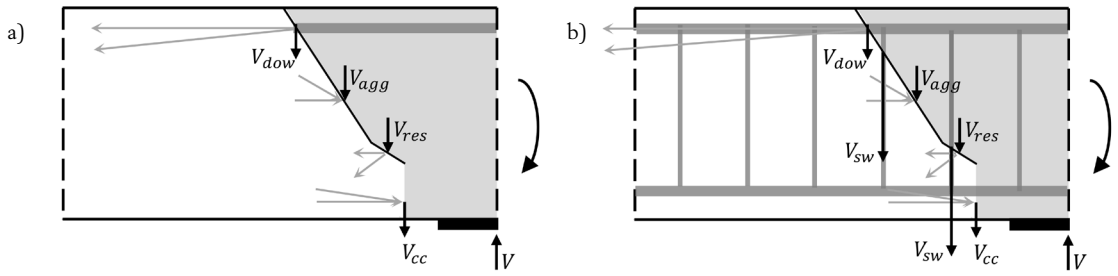

Fig. 8. (a) Shear-transfer actions in a specimen without shear reinforcement: aggregate interlock (V_{agg}), dowel action (V_{dow}), residual tensile strength (V_{res}) and inclination of the compression chord (V_{cc}); (b) shear-transfer actions in a specimen with shear reinforcement considering the contribution of the stirrups (V_{sw}).

specimens without shear reinforcement (B10 to B12), several shear-transfer actions on cracked concrete contribute to the shear strength (aggregate interlock, residual tensile strength of concrete, dowel action of the flexural reinforcement and contribution of the compression chord, see Figure 8a). For specimens with shear reinforcement (B1 to B9 and B13 to B15), the contribution of the stirrups to the shear strength has to be also considered (see Figure 8b).

In this work, the contribution of the shear reinforcement (V_S) and the contribution of the shear-transfer actions associated to the resistance of concrete (V_C) –accounting for the sum of the various shear-transfer actions related to concrete–to the shear strength of the specimens is investigated. The contribution of the shear reinforcement (V_S) is calculated following the procedure proposed by Campana *et al.* [19] and accounting for isolated DIC displacement measurements at stirrups location. The contribution associated to the concrete (V_C) is obtained as the difference between the total shear strength of the specimens and the contribution of the shear reinforcement (the various shear-transfer actions related to concrete was presented in detail in Monserrat López *et al.* [7]).

The development of the inclined critical shear crack (the crack leading to shear failure) leads to the activation of the stirrups intercepted by it and, as a result, shear forces can be carried by them. The sum of the shear force (V_{SW}) carried by each stirrup intercepted by the critical shear crack results in the contribution of the shear reinforcement (V_S) according to:

$$V_s = \sum V_{sw} = \sum 2\sigma_{sw} \frac{\phi^2 \pi}{4} \quad (1)$$

where ϕ is the diameter of the bar (stirrup with two branches) and σ_{sw} is the tensile stress of the stirrup, calculated following the procedure of Campana [19].

The tensile stress of a single stirrup (σ_{sw}) is obtained [19] from the isolated measurements of the critical shear crack openings performed by DIC. At the location where the critical shear crack (i) intercepts the stirrup, its vertical crack opening ($v_{sw,i}$) is obtained from the measured displacements of the concrete surfaces at two points (j and k) vertically aligned with the stirrup (Figure 9a). Before bar yielding, the constant bond stress is assumed [20] $\tau_{b1} = 2f_{ct}$ and, after yielding, it is reduced to $\tau_{b2} = 2f_{ct}$ to consider the decreasing bond stress due to the bar lateral contraction [21] (Figure 9b). On this basis, and by considering a bilinear stress-strain relationship with strain hardening for the steel (Figure 9c), the measured crack openings, the stresses (σ_{sw}) and strains (ε_{sw}) in a stirrup are determined (Figure 9d). The procedure neglects the concrete strains, so the crack opening ($v_{sw,i}$) is obtained by integrating the strains distribution (ε_{sw}) of a stirrup along the tributary length ($l_{cont,i}$) of the crack:

$$V_{sw,i} = \int_{l_{cont,i}} \varepsilon_{sw}(x)\, dx \quad (2)$$

For the specimens of the experimental programme, two stirrups are normally intercepted by the critical shear crack in specimens of series R1, and three in the case of specimens of series R2 (cracking patterns for all tests were presented in detail in Monserrat López *et al.* [7]). Those stirrups intercepted by the horizontal branch of the critical shear crack are not considered [19,22] and the accounted stirrups are yielded at shear failure, as small crack openings are sufficient to yield small bar diameters [19,22]. Table 3 presents the values of the vertical opening of the critical shear crack (i) at the location where it intercepts each stirrup ($v_{sw,i,S1}$, $v_{sw,i,S2}$ and $v_{sw,i,S3}$) at shear failure (only for series R1 and R2).

The values of the contribution of the shear reinforcement ($V_{s,R}$) and the contribution related to the concrete ($V_{c,R}$) to the shear strength of the specimens based on test results is presented in Table 4.

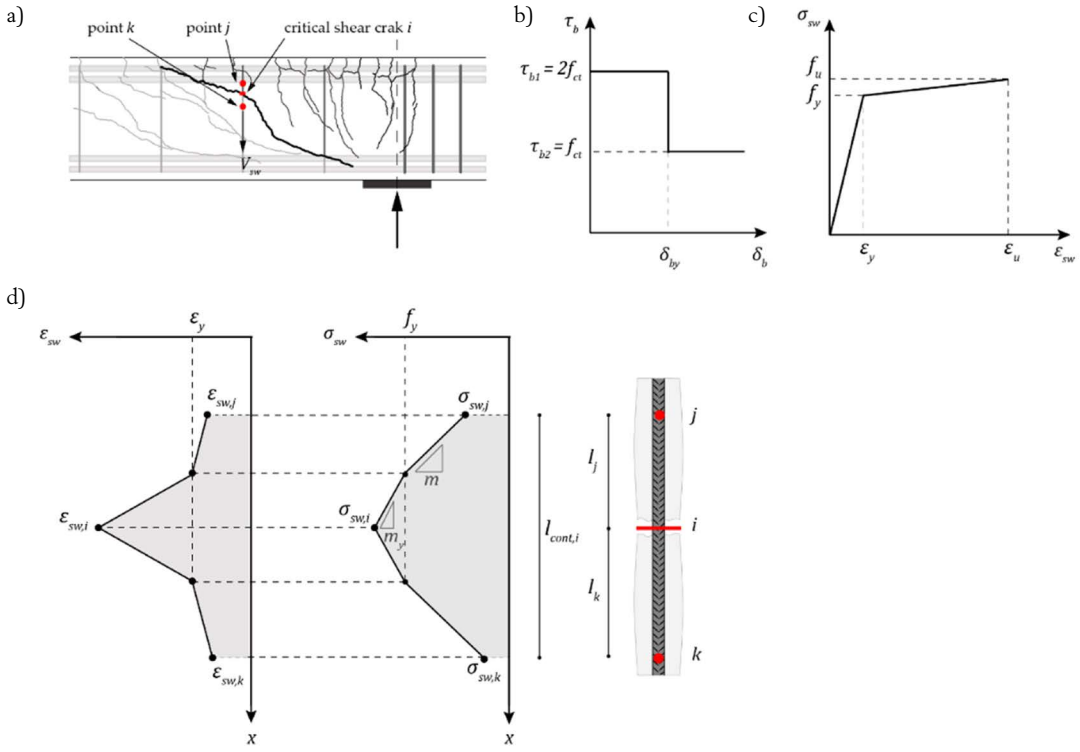

Figure 9. Shear reinforcement contribution: (a) obtaining the vertical crack opening of the critical shear crack by DIC; (b) the considered rigid-plastic bond behavior; (c) the considered bilinear hardening stress-strain relationship of steel (reinforcement steel properties in [6]) ; (d) transmission of stresses and strains in a stirrup [19].

TABLE 3.
Vertical opening of the critical shear crack at the location where it intercepts the stirrups at failure.

Specimen	Test	$v_{sw,i,S1}$ (mm)	$v_{sw,i,S2}$ (mm)	$v_{sw,i,S3}$ (mm)	Test	$v_{sw,i,S1}$ (mm)	$v_{sw,i,S2}$ (mm)	$v_{sw,i,S3}$ (mm)
B1	B1C-R1-S1-L1	4.06	5.20	-	B1S-R1-S1-L6	2.70	4.39	-
B2	B2C-R1-S2-L1	2.34	1.64	-	B2S-R1-S2-L6	0.39	0.60	-
B3	B3C-R1-S3-L1	1.57	1.78	-	B3S-R1-S3-L6	3.37	3.50	-
B4	B4C-R1-S1-L1.6	1.96	3.69	-	B4S-R1-S1-L5	3.23	3.36	-
B5	B5C-R1-S2-L1.6	2.04	3.13	-	B5S-R1-S2-L5	2.44	2.65	-
B6	B6C-R1-S3-L1.6	1.66	5.24	-	B6S-R1-S3-L5	1.09	1.71	-
B7	B7C-R1-S1-L2.3*	-	-	-	B7S-R1-S1-L4	0.97	2.19	-
B8	B8C-R1-S2-L2.3	2.70	1.80	-	B8S-R1-S2-L4	0.13	1.98	-
B9	B9C-R1-S3-L2.3	2.29	2.55	-	B9S-R1-S3-L4	1.05	3.12	-
B13	B13C-R2-S1-L1	2.16	3.18	2.19	B13S-R2-S1-L4	1.70	2.61	3.12
B14	B14C-R2-S2-L1	0.58	1.32	1.95	B14S-R2-S2-L4	0.49	1.52	1.50
B15	B15C-R2-S3-L1	2.19	1.27	1.68	B15S-R2-S3-L4	1.22	2.03	1.62

Note: V (shear failure); M (bending failure); A (after yielding); B (before yielding); PH (plastic hinge); shear at corresponding support section including self-weight; *test with different configuration [16].

4.2. Flexural and shear deformations

The analysis of flexural and shear deformations of the specimens is plotted in Fig. 10. The critical shear crack divides the specimens into two different bodies (one above the crack and other below it). The body above the critical shear crack only develops flexural deformation (accounted by the flexural rotation, ψ_f); whereas the body below the crack develops shear deformation as well linked to the development of the critical shear crack.

The kinematics of the critical shear crack (refers to Fig. 11a) can be explained by a rotational movement (shear crack rotation ψ_s, see Fig. 10) with the centre of rotations (CR) located near the tip of the crack [23,24] and a vertical displacement (shear displacement v_s see Fig. 10) between the lips of the crack that may be constant or not along the

TABLE 4.
Analysis of test results: calculated values at failure.

Specimen	Test	$V_{s,R}$ (kN)	$V_{c,R}$ (kN)	ψ_f (mrad)	ψ_t (mrad)	w (mm)	Test	$V_{s,R}$ (kN)	$V_{c,R}$ (kN)	ψ_f (mrad)	ψ_t (mrad)	w (mm)
B1	B1C-R1-S1-L1	123.7	73.1	10.6	ND	2.7	B1S-R1-S1-L6	121.2	18.2	36.4	37.2	3.1
B2	B2C-R1-S2-L1	118.1	96.5	3.5	ND	1.5	B2S-R1-S2-L6	111.7	30.7	35.3	39.7	0.8
B3	B3C-R1-S3-L1	116.7	89.6	8.9	ND	1.4	B3S-R1-S3-L6	124.0	21.2	53.8	59.6	1.9
B4	B4C-R1-S1-L1.6	118.3	55.9	11.6	17.9	1.9	B4S-R1-S1-L5	127.0	16.1	25.3	27.0	2.8
B5	B5C-R1-S2-L1.6	119.1	96.0	13.1	24.7	1.6	B5S-R1-S2-L5	119.7	69.0	46.2	51.7	2.0
B6	B6C-R1-S3-L1.6	120.1	87.6	14.4	20.2	3.4	B6S-R1-S3-L5	116.4	74.4	41.3	42.3	1.4
B7	B7C-R1-S1-L2.3*	-	-	-	-	-	B7S-R1-S1-L4	116.8	99.5	15.7	23.4	1.1
B8	B8C-R1-S2-L2.3	111.4	56.3	30.7	34.2	1.6	B8S-R1-S2-L4	96.7	104.2	22.4	27.6	0.8
B9	B9C-R1-S3-L2.3	112.4	36.3	26.4	28.4	1.4	B9S-R1-S3-L4	116.8	75.5	14.8	27.0	2.1
B10	B10C-R0-S1-L1	0.0	150.2	8.0	ND	3.0	B10S-R0-S1-L4	0.0	82.4	11.0	11.7	0.6
B11	B11C-R0-S2-L1	0.0	188.9	4.0	ND	2.5	B11S-R0-S2-L4*	0.0	92.0	22.3	24.5	0.5
B12	B12C-R0-S3-L1	0.0	120.8	7.9	ND	4.5	B12S-R0-S3-L4	0.0	87.6	7.6	8.9	0.5
B13	B13C-R2-S1-L1	176.2	58.8	8.7	ND	2.0	B13S-R2-S1-L4	175.3	42.3	22.0	24.1	1.9
B14	B14C-R2-S2-L1	171.9	95.9	8.5	ND	1.0	B14S-R2-S2-L4	172.0	50.5	23.9	30.5	1.3
B15	B15C-R2-S3-L1	174.0	107.0	11.0	ND	ND	B15S-R2-S3-L4	174.5	24.6	24.6	29.7	1.7

Note: *analysis not performed (bending failure); ND: no data available.

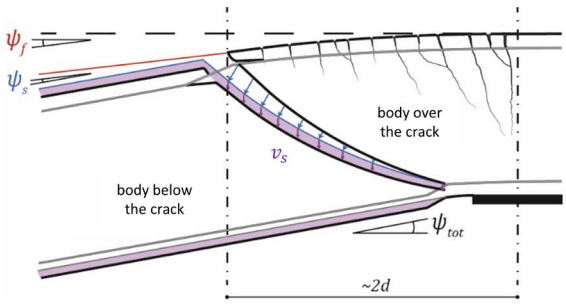

Figure 10. Flexural and shear deformations for the specimens: flexural rotation (ψ_f) and total rotation (ψ_t).

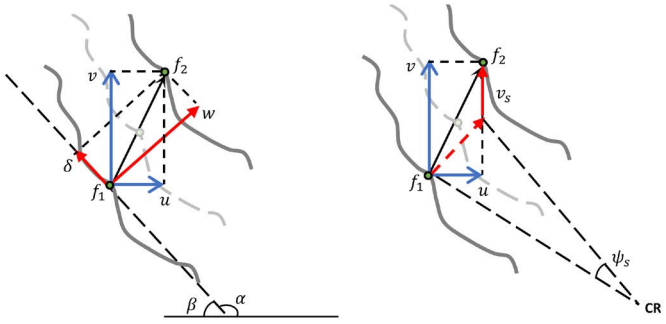

Figure 11. Critical shear crack kinematics: (a) simplification according to a rotation and a vertical displacement; (b) detailed crack opening and sliding.

crack (if it is not constant, it contributes to the rotation of the bottom fibres of the specimen) [25,26]. As a result, the total rotation ψ_t (see Figure 10) developed by the body below the critical shear crack is larger than the flexural one. This total rotation is obtained based on DIC measurements as the difference between the slope of the bottom fibres at the support section and the maximum slope at the end of the length of the specimen where the critical shear crack develops ($2d$).

Flexural rotation (ψ_f) represents the deformation of the specimens due to flexural stresses in an integrated way. At failure, the flexural rotations of the specimens are obtained by integrating the section curvature (χ) (estimated by the continuous measurements of the strains in the top and the bottom fibres performed by DIC) along the length of the specimen where the critical shear crack develops (Eq. 3). This length corresponds to the distance between the support section and the section at which the critical shear crack intercepts the flexural tensile reinforcement and it is approximately equal to $2d$ for all specimens.

$$\psi_f = \int_{2_d} \chi(x)\, dx \qquad (3)$$

The normalized shear force ($V/\sqrt{f_c}bd$) is plotted versus the flexural rotation (ψ_f) for the specimens of series R1 (ρ_w= 0.13%) and section S2 (ρ = 2.29%) in Figure 12. In cantilever tests (Figure 12a), it can be noted that the flexural rotation increases with increasing shear force until failure for specimens failed in shear before yielding of the flexural reinforcement (B2C-R1-S2-L1 and B5C-R1-S2-L1.6), while this rotation increases under constant shear force after yielding until shear failure for the specimen B8C-R1-S2-L2.3. In continuous beam tests (Figure 12b), it is observed that the flexural rotation increases with increasing shear force until failure for the specimen failed in shear after the formation of the first plastic hinge (B2S-R1-S2-L6); however, shear failure occurs under increasing flexural rotation and constant shear force for specimens failed after the formation of second plastic hinge (B5S-R1-S2-L5 and B8S-R1-S2-L4).

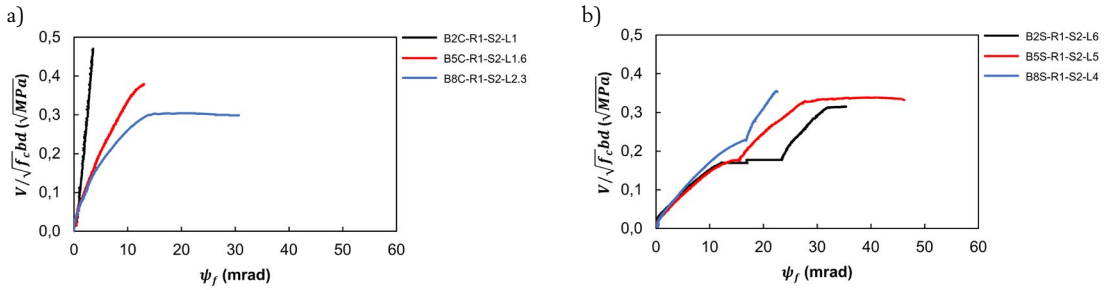

Figure 12. Normalized shear force *versus* flexural rotation for the specimens of series R1 and section S2: (a) cantilever tests; (b) continuous beam tests.

On the other hand, the development of inclined cracking (resulting in the critical shear crack leading to shear failure) evidences the deformation of the specimens due to shear stresses. Based on the displacement measurements of cracking performed by DIC [18] and following the procedure proposed by Campana *et al.* [19], the kinematics of the critical shear crack is obtained for all specimens. This kinematics (which involves relative horizontal -*u*- and vertical -*v*- displacements of the crack lips) can be explained by a crack opening normal to the crack (w) and a sliding (δ) tangential to the crack according to [19] (refers to Figure 11b):

$$\vec{w}=\begin{bmatrix}\delta\\ w\end{bmatrix}=\begin{bmatrix}\cos\alpha & \sin\alpha\\ -\sin\alpha & \cos\alpha\end{bmatrix}\begin{bmatrix}u\\ v\end{bmatrix} \quad (4)$$

The kinematics of the critical shear crack obtained from various cantilevers tests and continuous beam tests for specimens without shear reinforcement (series R0) and with shear reinforcement (series R1 and R2) is plotted in Figure 13. This kinematics is represented at various step loads: previous to the shear failure ($V<V_R$), at shear failure just prior to the collapse of the specimen ($V=V_R$, the red point indicates this

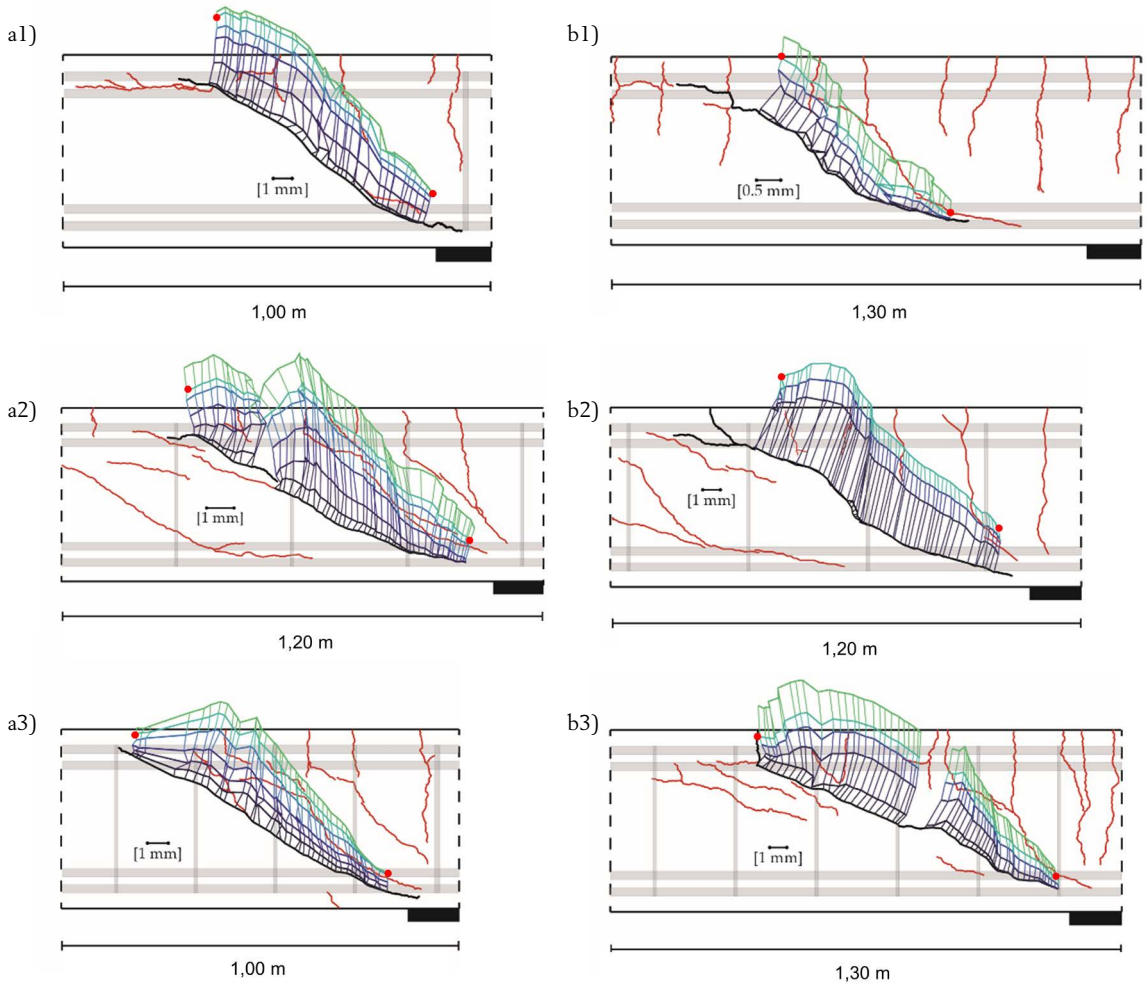

Figure 13. Kinematics of the critical shear crack (the red point indicates the step load corresponding to the shear failure): (a) cantilever tests -(a1) B10C-R0-S1-L1; (a2) B4C-R1-S1-L1.6; (a3) B13C-R2-S1-L1-; (b) continuous beam tests -(b1) B10S-R0-S1-L4; (b2) B1S-R1-S1-L6; (b3) B13S-R2-S1-L4-.

step load), and subsequent to the shear failure ($V<V_R$ corresponding to the drop of the load due to the collapse of the specimen).

The values of the flexural rotation, of the total rotation and of the critical shear crack opening (average values of the crack opening corresponding to the different points of the polyline defining the crack) at failure for all specimens are summarized in Table 4.

4.3. Shear-flexural rotation interaction

The normalized shear strength associated to concrete ($V_{c,R}/\sqrt{f_c}bd$)) –accounting for the sum of the various shear-transfer actions related to concrete and obtained as the difference between the total shear strength and the contribution of the shear reinforcement at failure calculated according to Eq. 1)– is plotted versus the flexural rotation (ψ_a) at failure in Figure 14a and versus the critical shear crack opening (w) at failure in Figure 14b for all specimens. It can be noted that the shear strength associated to concrete reduces for increasing flexural rotations (Figure 14a). This result evidences that the shear strength of the specimens is governed by the flexural strains developed. Nevertheless, it must be pointed out that the shear strength associated to concrete is not influenced by the crack opening for the tested specimens (14b). That is, the shear strength does not necessarily decrease for increasing crack openings. Although the increase of crack opening can entail a reduction of some shear-transfer actions (such as aggregate interlock) [3,4], it also can mean the activation of some others (such as dowel action), which results in an increase of the shear strength associated to the sum of the shear-carrying mechanisms related to concrete (a detailed analysis of the influence of the various shear-carrying mechanisms on the shear strength was presented in Monserrat López [27]).

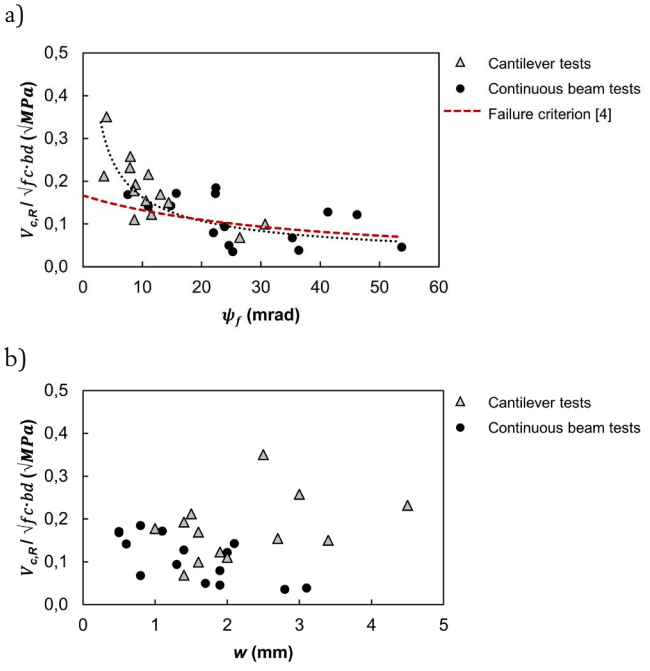

Figure 14. Normalized shear strength related to concrete for all specimens *versus*: (a) flexural rotation; (b) crack opening.

The reduction of the shear strength related to concrete for increasing flexural rotations occurs both for cantilever tests and continuous beam tests (Figure 14a). Generally, the later develop larger flexural strains (large flexural rotations) than the former and, as a consequence, the shear strength in continuous beams is more limited than in cantilever tests. In fact, the reduction of the shear strength until shear failure for increasing plastic strains in continuous beam tests (failure always occurs after yielding of the flexural reinforcement) evidences that the flexural deformation influences the shear behavior of the specimens beyond the yielding point. In addition, the shear-flexural rotation interaction on the tested specimens is common to specimens without and with shear reinforcement. That is, the shear strength related to concrete decreases for increasing flexural rotations regardless of the presence or absence of stirrups.

The loss of shear strength for increasing values of rotation after yielding of the flexural reinforcement was already confirmed by the experimental programme conducted by Vaz Rodrigues *et al.* [4] on statically determinate reinforced concrete beams without stirrups. The experimental results allowed formulating a shear failure criterion (refer to Figure 14a) according to the rotation for reinforced concrete members without shear reinforcement based on the Critical Shear Crack Theory (CSCT) [3].

Therefore, this experimental study [4] has already proved the influence of the flexural deformation on shear strength for statically determinate specimens without stirrups; however, the tests included in the present work allow extending the analysis of this phenomenon for statically determinate and indeterminate specimens without and with stirrups. This extended analysis evidences the reduction of the shear strength for increasing flexural rotations for statically determinate and indeterminate reinforced concrete members without and with shear reinforcement that reach shear failures before and after yielding of the flexural reinforcement (Figure 14a).

4.4. Influence of the tensile flexural reinforcement on the shear-flexural rotation interaction

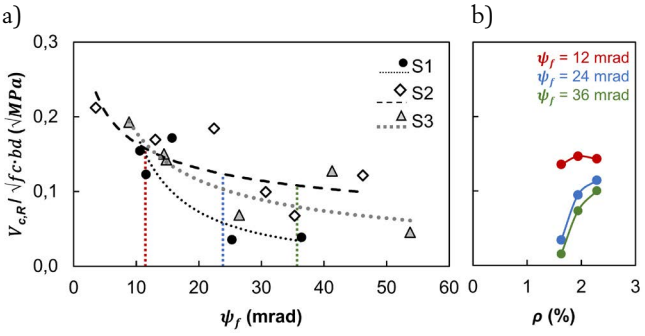

Note: B7C-R1-S1-L2.3 - analysis not performed (bending failure).

Figure 15. Influence of the flexural reinforcement on the moment-shear interaction: (a) normalized shear strength related to concrete according to the flexural rotation for the specimens of series R1; (b) normalized shear strength related to concrete according to flexural reinforcement ratio for three different levels of flexural rotation.

The influence of the flexural reinforcement on the shear-flexural rotation interaction (represented by the loss of shear

strength related to concrete – $V_{c,R}/\sqrt{f_c}bd$ – for increasing flexural rotations – ψ_f –) for the specimens of series R1 (ρ_w = 0.13%) is plotted in Figure 15a. It can be noted that for the same value of flexural rotation, the larger the flexural reinforcement ratio, the greater the shear strength for the tested specimen. In other words, depending on the flexural reinforcement of the section (sections S1, S2 and S3), the tested specimens reach the same shear strength under different levels of flexural rotation. In addition to this, it is observed that the increase of shear strength related to concrete with flexural reinforcement ratio for the same level of rotation is more significant as the flexural rotation increases. On this point, Figure 15b represents for three different levels of flexural rotation (12, 24 and 36 mrad) the values of the normalized shear strength related to concrete ($V_{c,R}/\sqrt{f_c}bd$) versus the flexural reinforcement ratio of the sections S1 (ρ = 1.63%), S2 (ρ = 2.29%) and S3 (ρ = 1.94%) for the series R1 (ρ_w = 0.13%). It can be noted that the increase in shear strength for increasing flexural reinforcement ratios is more significant for larger rotations. While for a flexural rotation of 12 mrad, the shear strength related to concrete is almost the same independent of the flexural reinforcement; for larger values of flexural rotation (24 and 36 mrad), the shear strength provided by concrete considerably increases with flexural reinforcement ratio.

4.5. Influence of the shear reinforcement on the shear-flexural rotation interaction

On the other hand, the influence of the shear reinforcement on the shear-flexural rotation interaction for the specimens of series R0 (without stirrups), R1 (ρ_w = 0.13%) and R2 (ρ_w = 0.20%) is plotted in Figure 16. It can be noted that for the same value of flexural rotation, the larger the shear reinforcement ratio, the lower the shear strength related to concrete for the tested specimen. This result evidences that, whereas the shear strength of the specimens increases for larger shear reinforcement ratios (see Table 2), the contribution to that resistance of the various shear-transfer mechanisms related to concrete decreases. This phenomenon is represented in Figure 17, where the normalized shear strength ($V_{c,R}/\sqrt{f_c}bd$) (Figure 17a) and the normalized shear strength related to concrete ($V_{c,R}/\sqrt{f_c}bd$) (Figure 17b) are plotted versus the shear reinforcement ratio (series R0, R1 and R2) for comparable tests (cantilever tests L1 and continuous beam tests L4, see Table 1). It is also observed in Figure 17 that, for the same amount of shear reinforcement, cantilever tests reach larger values of shear strength than continuous beam tests, although a greater scatter. The limited scatter of continuous beam tests (compared to cantilever tests) can be explained by the reduced contribution of the dowel action to shear strength due to the yielding of the tensile flexural reinforcement in continuous beam tests [7,28]. For cantilever tests, the contribution of the dowel action to the shear strength is considerable [7] and, apart from the kinematics of the critical shear crack, it depends on the amount of flexural reinforcement. Considering that the tested specimens have different amounts of this reinforcement according to three series (S1, S2 and S3), the scatter in cantilever tests may be explained. However, for continuous beam tests, the yielding of the flexural reinforcement before the shear failure limits the contribution of the dowel action and, as a result, the scatter associated with the different flexural reinforcement ratios (S1, S2 and S3) is also limited.

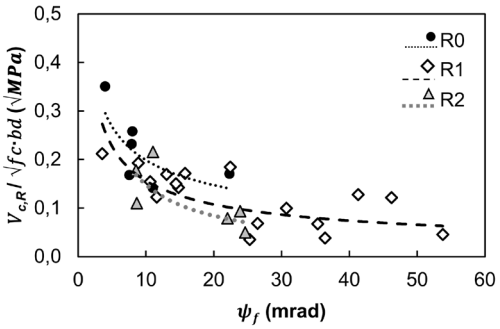

Note: B7C-R1-S1-L2.3 - analysis not performed (bending failure).

Figure 16. Influence of the shear reinforcement on the moment-shear interaction: normalized shear strength related to concrete according to the flexural rotation for the specimens of series R0, R1 and R2.

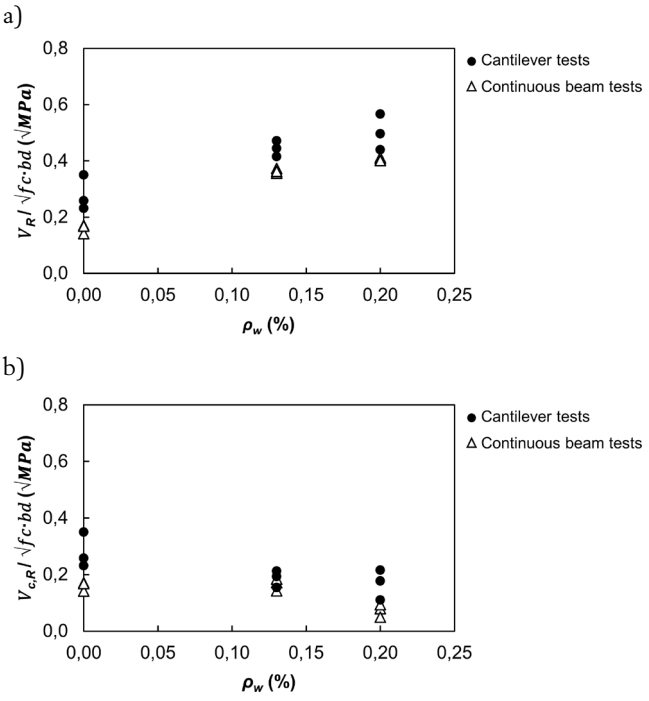

Figure 17. Influence of the shear reinforcement on the shear strength for cantilever tests L1 and continuous beam tests L4: (a) normalized shear strength; (b) normalized shear strength related to concrete.

4.6. Comparison of the test results with existing code provisions

The experimental-to-predicted shear strength ($V_{R,test}/V_{R,calc}$) ratio is plotted versus the flexural rotation (ψ_f) at failure for all test in Figure 18 (statistics of the ratio are included). Only cantilever tests with shear failure before yielding of the flexural reinforcement (failure mode V(B), see Table 2) and continuous beam tests with shear failure after the development of first plastic hinge (failure mode V(1PH), see Table 2) are included in the analysis. The predicted shear strength is obtained for ACI 318-19 [11] (Figure 18a), EC-2 [12] (Figure 18b) and MC2010 [15] (LoA-I in Figure 18c and LoA-III in Figure 18d). In all cases, the partial safety factor for concrete material properties is considered equal to one and the angle between web compression and the axis of the member is the minimum.

Regarding the different code provisions for specimens without and with shear reinforcement, the scatter of the experimental-to-predicted shear strength ratio is always greater for test results of specimens without shear reinforcement (series R0) than for those of specimens with stirrups (series R1 and R2). This reflects the larger variability of the phenomena governing the shear strength for members without shear reinforcement than for those with it.

The provisions of shear strength differ considerably depending on whether the formulation of the design code accounts for the reduction of shear strength resulting from the development of flexural deformations in the flexural reinforcement. In this regard, the predicted ratio $V_{R,test}/V_{R,calc}$ plotted in Figure 18 versus the flexural rotation allow identifying the capability of each design codes to capture the dependence between shear strength and flexural deformation (accounted by the flexural rotation). The formulation provided by ACI 318-19, EC-2 and MC2010 LoA-I does not directly include a reduction of the shear strength because of the development of flexural deformations (see the trend plotted in Figure 18a, 18b and 18c). Shear strength provisions in these cases show similar scatter values: 33~36% for specimens without stirrups and 11~16% for specimens with stirrups. However, the shear strength values predicted by MC2010 LoA-I are much more conservative (average of the ratio $V_{R,test}/V_{R,calc}$) equal to 1,94 for specimens without stirrups and 1,67 for specimens with stirrups) than those predicted by ACI 318-19 (1,23 and 1,11, respectively) and EC-2 (1,01 and 1,17, respectively). On the other hand, the iterative formulation provided by MC2010 LoA-III (based on the MCFT [13,14]) accounts for the moment-shear interaction by reducing shear strength according to the strains of the flexural reinforcement (see the trend plotted in Figure 18d) and it improves the shear strength LoA-I predictions. In all cases, the shear strength values predicted by MC2010 LoA-III (LoA-II for series R0) are lower than the experimental values obtained in tests ($V_{R,test}/V_{R,calc} > 1$). The average of the ratio $V_{R,test}/V_{R,calc}$ is 1,37 and 1,18 for specimens without and with stirrups, respectively, and the scatter of this ratio is the lowest (15% and 8% for specimens without and with stirrups, respectively). It must be pointed out that the reduction of shear strength is bounded because of flexural deformations in MC2010 LoA-III are limited to the yielding strain of the longitudinal tension reinforcement, since they are derived from a sectional analysis by assuming a linear elastic stress-strain relationship for the steel.

5. SHEAR STRENGTH REDUCTION ACCOUNTING FOR THE PLASTIC ROTATION DEMAND OF THE PLASTIC HINGES

The reduction of the shear strength of reinforced concrete members for increasing flexural rotations has been confirmed. It has also been proved that this reduction of the shear resistance extends for increasing rotations of the plastic

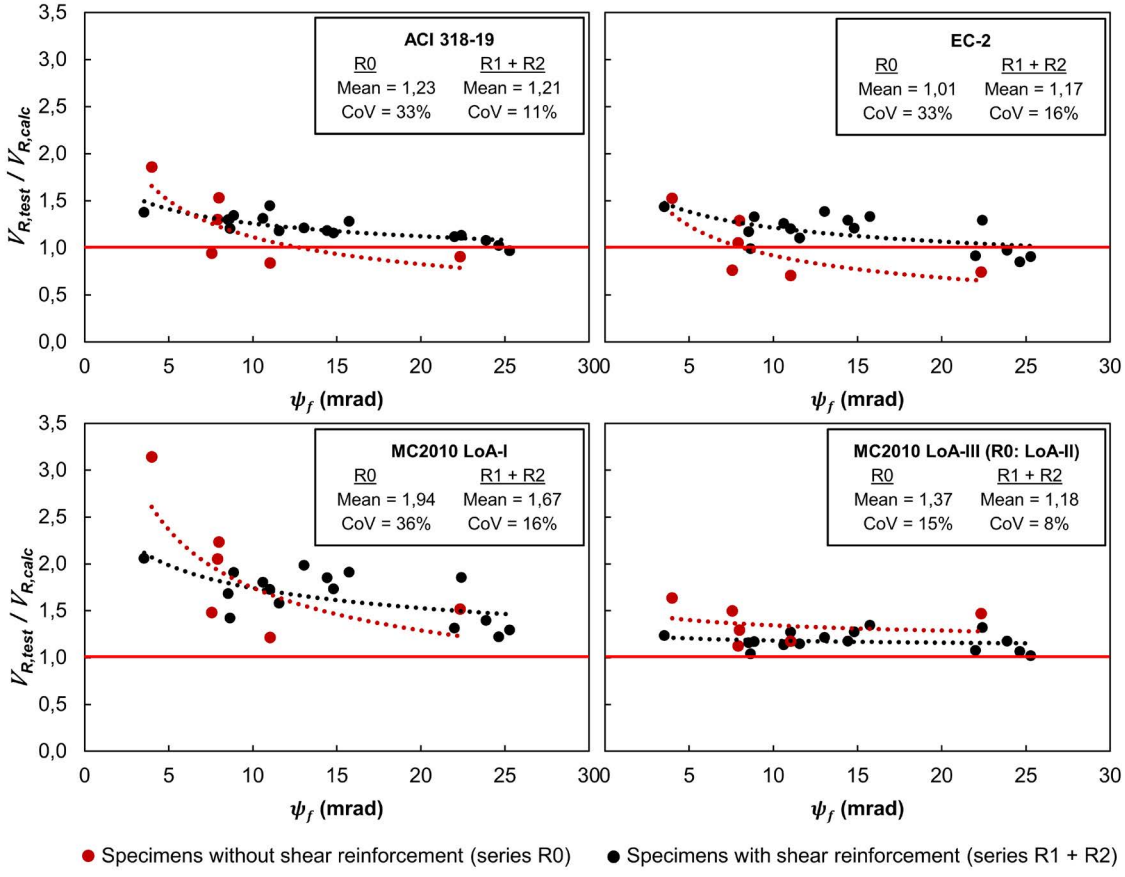

Figure 18. Experimental-to-predicted shear strength ratio versus flexural rotation for different design code provisions (ACI 318-19, EC-2, MC2010 LoA-I and MC2010 LoA-III) for specimens without and with shear reinforcement.

hinges after yielding of the flexural reinforcement. That is, the rotation demand of a plastic hinge for increasing loads after yielding involves a reduction of its shear strength. In statically indeterminate structures, these increasing loads also lead to increasing shear forces at the plastic hinge. When these shear forces reach the shear failure criterion, the shear capacity of the plastic hinge is reached. A simple procedure to calculate the shear capacity of a plastic hinge after yielding of the flexural reinforcement is linearizing the shear failure criterion considering the tangent to the shear failure criterion at the shear strength $V_R\,(\psi_y)$ calculated for the rotation corresponding to the yielding of the flexural reinforcement (ψ_y) (see line r_2 in Figure 19) according to Eq. 5. The linearization of the shear failure criterion [4] provides a safe estimate of the shear strength as the failure criterion is concave (see Figure 14a).

$$V_R = V_R(\psi_R) - k_\psi(\psi - \psi_y) \tag{5}$$

where $k_\psi = -\left[\frac{dV_R(\psi)}{d\psi}\right]_{\psi_y}$ is the slope (negative) of the line r_2 (see Figure 19).

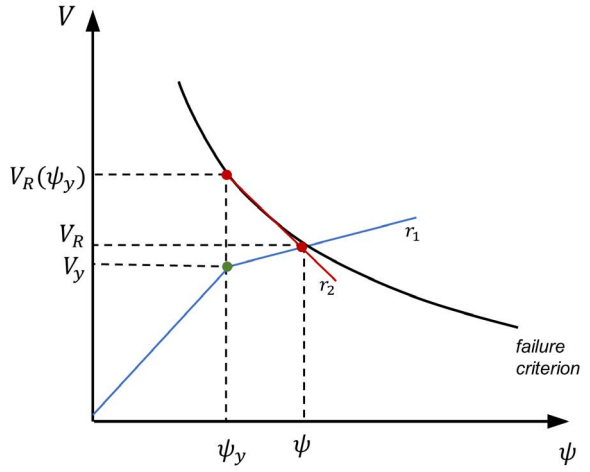

Figure 19. Shear strength of reinforced concrete members without shear reinforcement versus flexural rotation.

The expression of Eq. 5 shows that the shear strength of a plastic hinge can be calculated by considering the shear strength at yielding strain of the flexural tensile reinforcement reduced by a term that depends on the plastic rotation demand of the plastic hinge. This reduction will be small for low values of k_ψ, which corresponds to shear failures with large flexural rotations, according to the failure criterion (see Figure 19).

On the other hand, the plastic rotation demand of a plastic hinge ($\psi - \psi_y$) can be expressed as a linear function of the applied shear forces according to (see line r_1 in Figure 19):

$$\psi - \psi_y = \frac{1}{k_\theta}(V_E - V_y) \tag{6}$$

where k_θ is the slope of the line r_1 (see Figure 19) and depends on the geometrical and mechanical characteristics of the structure and V_y is the shear force applied for yielding of the flexural reinforcement.

The shear strength of a plastic hinge will be reached when the shear force reaches the shear failure criterion ($V_E = V_R$). Thus, from Eq. 5 and 6, it follows that:

$$V_R = \frac{k_\theta V_R(\psi_y) - k_\psi V_y}{k_\theta - k_\psi} \tag{7}$$

For the calculation of $V_R\,(\psi_y)$, the failure criterion for reinforced concrete members without shear reinforcement proposed by Vaz Rodrigues *et al.* [4] (refer to Figure 14a) may be assumed. For members with stirrups, the shear resistance may be considered as the sum of the shear strength provided by concrete and the shear force resisted by the stirrups intercepted by the critical shear crack ($V_{s,R}$) according to:

$$V_R(\psi_y) = \frac{1}{6}\frac{bd\sqrt{f_c}}{1+2\frac{\psi_y d}{d_g}} + V_{s,R}(\psi_y) \tag{8}$$

Considering the failure criterion proposed by Vaz Rodrigues *et al.* [4] (refer to Figure 14a), the value of k_ψ is thus given by:

$$k_\psi = -\left[\frac{dV_R(\psi)}{d\psi}\right]_{\psi_y} = 2\frac{d}{d_g}\frac{V_R(\psi_y)}{1+2\psi_y\frac{d}{d_g}} \tag{9}$$

The shear force resisted by stirrups intercepted by the critical shear crack is the sum of the individual forces of the stirrups $V_{s,R} = \sum(2\pi\phi^2/4)\,\overline{\sigma_{sw}}$. Assuming an average stress $\overline{\sigma_{sw}}$ for these stirrups at shear failure and that this crack extends along the shear crack ($d\cdot\cot\theta$), the shear force resisted by stirrups can be obtained as:

$$V_{s,R}(\psi \geq \psi_y) = \frac{2\pi\phi^2}{4}\overline{\sigma_{sw}}\frac{d\cot\theta}{s} \tag{10}$$

where ϕ is the diameter of the bar (stirrup with two branches) and s is the spacing of the shear reinforcement. For the tested specimens, $\overline{\sigma_{sw}} = f_y$ as the stirrups yielded and $\cot(\theta)=2$.

The shear strength predicted by the proposed simplified method shows good agreement with the results obtained from the continuous beam tests carried out in this work. The average value of the ratio between the experimental shear strength (refer to Table 2) and the estimated shear strength (refer to Eq. 7) considering all the continuous beam tests (15 tests) is 1.06 (CoV = 11.7%) (see Figure 20).

For reduced plastic rotation demands -that is, large k_θ leading to a slope of line r_1 quite vertical (see Figure 19)-, the shear strength of the plastic hinge is close to the shear resistance $V_R(\psi_y)$ calculated for the yielding of the flexural reinforcement. This is the case of beams with high sectional stiffness. Conversely, for large plastic rotation demands - that is, limited k_θ leading to a slope of line r_1 quite horizontal (see Figure 19)-, the shear strength of the plastic hinge is close to the shear force applied for yielding of the flexural reinforcement (V_y).

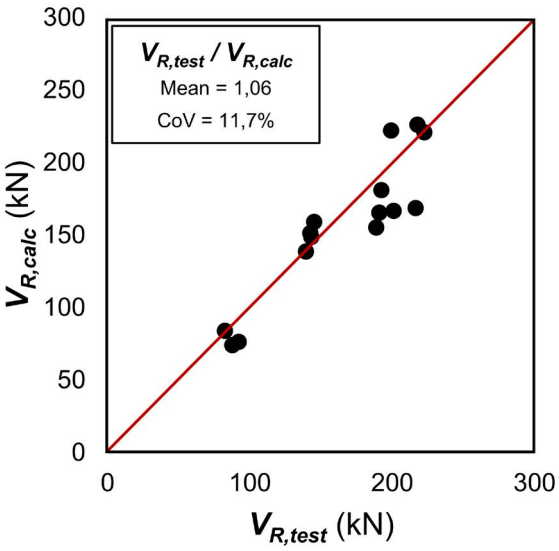

Figure 20. Shear strength for all continuous beam tests: experimental values and estimated values according to the proposed simplified method.

6. CONCLUSIONS

- The test system allowed reproducing shear failures of statically determinate and indeterminate structures on the tested specimens namely cantilever tests and continuous beam tests, respectively. In continuous beam tests, the tested specimens failed in shear after yielding of the flexural reinforcement due to the reduction of the shear strength capacity because of increasing plastic deformation (flexural rotation).
- Digital image correlation (DIC) technique has proved to be a powerful tool to perform displacement measurements on specimens. The employment of this technique allows the kinematics of the critical shear crack to be obtained in detail, as well as the rotations developed throughout the length of the specimen where this crack develops.
- The critical shear crack divides the specimen into two bodies. The body over this crack develops flexural deformation (flexural rotation), whereas the body below it develops both flexural and shear deformations. As a result, the total rotation measured in the bottom fibres of the specimen is larger than the flexural one. This difference between the flexural and the total rotation is attached to the rotations developed by the critical shear crack.
- Flexural rotation and critical shear crack width represent flexural and shear deformations developed by specimens, respectively. These two parameters are used to analyse the effect of both deformations on the contribution of the various shear-transfer actions related to concrete to the shear strength of the specimens.
- Shear strength provided by concrete decreases for increasing values of flexural rotation, both for specimens with and without shear reinforcement. The results confirm that even after yielding of the flexural reinforcement the plastic flexural rotation reduces the shear strength capacity.
- Shear strength provided by concrete is not influenced by critical shear crack width. Although the increase of this width can entail a reduction of some shear-transfer actions, it also can mean the activation of some others and, as a result, an increase of the overall shear strength associated to the sum of the shear-carrying mechanisms related to concrete.
- The reduction of shear strength provided by concrete for increasing values of bending rotation is influenced both by flexural reinforcement and shear reinforcement ratios. Although shear strength increases for increasing shear reinforcement ratios, concrete contribution decreases as this ratio increases.
- It has been experimentally verified that the shear failure criterion proposed by Vaz Rodrigues *et al.* [4] is applicable to shear failures with plastic deformations of the flexural reinforcement both in members with and without shear reinforcement.
- An expression to obtain the shear strength of a plastic hinge has been proposed by linearizing a shear failure criterion formulated as a function of the flexural rotation. To this aim, the failure criterion proposed by Vaz Rodrigues *et al.* [4] is considered because of its simplicity. However, this proposal could be improved by including the influence of the flexural and shear reinforcement on the shear strength provided by concrete.

Acknowledgements

This research was funded with grants from the Ministerio de Economía y Competitividad (Spain) with Research Project BIA2015-64672-C4-4-R. Andrea Monserrat was particularly supported by the Conselleria d'Educació, Investigació, Cultura i Esport of the Generalitat Valenciana (Order 6/2015, DOCV no. 7615 15.09.2015) funded with European Regional Development Funds (ERDF) as a pre-doctoral researcher and by the Ministerio de Universidades (Spain) with the Recovery, Transformation and Resilience Plan (RD 289/2021 and order UNI/551/2021) funded by NextGenerationEU as a post-doctoral researcher. The experimental programme was developed in the Laboratory of Concrete of the Institute of Concrete Science and Technology (ICITECH) of the Universitat Politècnica de València (UPV). VIC2D software was employed during the research stay of Andrea Monserrat at the EPFL (Lausanne, Switzerland).

References

[1] K.-H. Reineck, E. C. Bentz, B. Fitik, D. A. Kuchma, and O. Bayrak, ACI-DAfStb Database of shear tests on slender reinforced concrete beams without stirrups, ACI Struct. J. 110 (2013) no. 5 867–876. https://doi.org/10.14359/51685839

[2] K.-H. Reineck, E. Bentz, B. Fitik, D. A. Kuchma, and O. Bayrak, ACI-DAfStb Databases for shear tests on slender reinforced concrete beams with stirrups," ACI Struct. J. 111 (2014) no. 5 1147–1156. https://doi.org/10.14359/51686819

[3] A. Muttoni and M. Fernández Ruiz, Shear strength of members without transverse reinforcement as function of critical shear crack width, ACI Struct. J. 105 (2008) no. 2 163–172. https://doi.org/10.14359/19731

[4] R. Vaz Rodrigues, A. Muttoni, and M. Fernández Ruiz, Influence of shear on rotation capacity of reinforced concrete members wi-

thout shear reinforcement, ACI Struct. J. 107 (2010) no. 5 516–525. https://doi.org/10.14359/51663902

[5] A. Monserrat López, P. Miguel Sosa, J. L. Bonet Senach, and M. Á. Fernández Prada, Influence of the plastic hinge rotations on shear strength in continuous reinforced concrete beams with shear reinforcement, Eng. Struct. 207 (2020). https://doi.org/10.1016/j.engstruct.2020.110242

[6] A. Monserrat López, P. Miguel Sosa, J. L. Bonet Senach, and M. Á. Fernández Prada, Experimental study of shear strength in continuous reinforced concrete beams with and without shear reinforcement, Eng. Struct. 220 (2020). https://doi.org/10.1016/j.engstruct.2020.110967

[7] A. Monserrat López, M. Fernández Ruiz, and P. Miguel Sosa, The influence of transverse reinforcement and yielding of flexural reinforcement on the shear-transfer actions of RC members, Eng. Struct. 234 (2021). https://doi.org/10.1016/j.engstruct.2021.111949

[8] J. Schlaich, K. Shafer, and M. Jennewein, Toward a consistent design of structural concrete, PCI J. 32 (1987) 74–150. https://doi.org/10.15554/pcij.05011987.74.150

[9] J. Schlaich and K. Schäfer, Design and detailing of structural concrete using strut-and-tie models, Struct. Eng. 69 (1991) no. 6 113–125.

[10] A. Muttoni, J. Schwartz, and B. Thürlimann, Design of Concrete Structures with Stress Fields, Birkhaüser / Springer, 1997.

[11] ACI Committee 318, Building code requirements for structural concrete (ACI 318-19); and commentary (ACI 318R-19), American Concrete Institute, 2019.

[12] CEN, EN 1992-1-1:2004, Eurocode 2: Design of concrete structures – Part 1-1: General rules and rules for buildings, European Committee for Standardization, 2004.

[13] F. J. Vecchio and M. P. Collins, The Modified Compression-Field Theory for reinforced concrete elements subjected to shear, J. Proc. 83 (1986) no. 2 219–231.

[14] E. Bentz, F. J. Vecchio, and M. P. Collins, Simplified Modified Compression Field Theory of calculating shear strength of reinforced concrete elements, ACI Struct. J. 103 (2006) no. 4 614–624. https://doi.org/10.14359/16438

[15] Fédération International du Béton (fib), Model Code 2010, Ernst & Sohn, 2012.

[16] X.-B. D. Pang and T. T. C. Hsu, Behavior of reinforced concrete membrane elements in shear, ACI Struct. J. 92 (1995) no. 6 665–679. https://doi.org/10.14359/9661

[17] X.-B. D. Pang and T. T. C. Hsu, Fixed-Angle Softened-Truss Model for reinforced concrete, ACI Struct. J. 93 (1996) no. 2 197–207. https://doi.org/10.14359/1452

[18] Correlated Solutions, Vic-2D Reference Manual, 2009.

[19] S. Campana, M. Fernández Ruiz, A. Anastasi, and A. Muttoni, Analysis of shear-transfer actions on one-way RC members based on measured cracking pattern and failure kinematics, Mag. Concr. Res. 65 (2013), no. 6 386–404. https://doi.org/10.1680/macr.12.00142

[20] V. Sigrist, Zum Verformungsvermögen von Stahlbetonträgern (Deformation capacity of reinforced concrete beams), ETH Zürich, 1995.

[21] M. Fernández Ruiz, A. Muttoni, and P. G. Gambarova, Analytical modeling of the pre- and postyield behavior of bond in reinforced concrete, J. Struct. Eng. 133 (2007) no. 10 1364–1372. https://doi.org/10.1061/(ASCE)0733-9445(2007)133:10(1364)

[22] P. Huber, T. Huber, and J. Kollegger, Investigation of the shear behavior of RC beams on the basis of measured crack kinematics, Eng. Struct. 113 (2016) 41–58. https://doi.org/10.1016/j.engstruct.2016.01.025

[23] M. Fernández Ruiz, A. Muttoni, and J. Sagaseta, Shear strength of concrete members without transverse reinforcement: A mechanical approach to consistently account for size and strain effects, Eng. Struct. 99 (2015) 360–372. https://doi.org/10.1016/j.engstruct.2015.05.007

[24] F. Cavagnis, M. Fernández Ruiz, and A. Muttoni, A mechanical model for failures in shear of members without transverse reinforcement based on development of a critical shear crack, Eng. Struct. 157 (2018) 300–315. https://doi.org/10.1016/j.engstruct.2017.12.004

[25] J. T. Simões, M. Fernández Ruiz, and A. Muttoni, Validation of the Critical Shear Crack Theory for punching of slabs without transverse reinforcement by means of a refined mechanical model, Struct. Concr. 19 (2018) no. 1 191–216. https://doi.org/10.1002/suco.201700280

[26] A. Muttoni, M. Fernández Ruiz, and J. T. Simões, The theoretical principles of the critical shear crack theory for punching shear failures and derivation of consistent closed-form design expressions, Struct. Concr. 19 (2018) no. 1 174–190. https://doi.org/10.1002/suco.201700088

[27] A. Monserrat López, Comportamiento frente a cortante de vigas continuas de hormigón armado: estudio experimental de los mecanismos resistentes y de la influencia de la cinemática desarrollada en combinación con los esfuerzos de flexión, Universitat Politècnica de València, 2020.

[28] F. Cavagnis, M. Fernández Ruiz, and A. Muttoni, An analysis of the shear-transfer actions in reinforced concrete members without transverse reinforcement based on refined experimental measurements, Struct. Concr. 19 (2018) no. 1 49–64. https://doi.org/10.1002/suco.201700145